Reactor-scale models for rf diode sputtering of metal thin films

S. Desa,[a] S. Ghosal, R. L. Kosut, J. L. Ebert, T. E. Abrahamson, and A. Kozak
SC Solutions, Santa Clara, California 95054

D. W. Zou, X. Zhou, J. F. Groves, and H. N. G. Wadley
University of Virginia, Charlotte, Virginia 22903

(Received 12 October 1998; accepted 29 March 1999)

This article describes the development of an integrated physical model for the rf diode sputtering of metal thin films. The model consists of: (1) a computational fluid dynamic finite element model for the velocity and pressure distribution of the working gas Ar flow in the chamber, (2) a steady-state plasma model for the flux and energy of Ar ions striking the target and the substrate, (3) a molecular dynamics sputtering model for the energy distribution, angle distribution, and yield of the sputtered atoms (Cu) from the target, and (4) a direct simulation Monte Carlo (DSMC) model for the transport of Cu atoms through the low-pressure argon gas to the deposition substrate. The individual models for gas flow, plasma discharge, Cu sputtering, and DSMC-based Cu atom transport are then integrated to create a detailed, steady-state, input–output model capable of predicting thin-film deposition rate and uniformity as a function of the process input variables: power, pressure, gas temperature, and electrode spacing. Deposition rate and uniformity in turn define the characteristics of thin films exploited in applications, for example, the saturation magnetic field for a giant magnetoresistive multilayer. This article also describes the development of an approximate input–output model whose CPU time is several orders-of-magnitude faster than that of the detailed model. Both models were refined and validated against experimental data obtained from rf diode sputtering experiments. © *1999 American Vacuum Society.* [S0734-2101(99)16204-3]

I. INTRODUCTION

The development, computational implementation, and integration of the appropriate physical models for rf diode sputtering, calibrated and refined using appropriate experimental results, can be used to effectively reduce time consuming and costly trial-and-error in the design, operation, and control of deposition systems for the fabrication of reliable, high-quality metal thin films. Therefore, we describe the development and subsequent integration of reactor-scale models for the primary physical phenomena—gas flow, plasma discharge, sputtering and atom transport—constituting rf diode sputtering/deposition for fabricating thin metal films, for example, those exhibiting giant magnetoresistance (GMR). The resulting integrated input–output model is capable of predicting thin-film deposition rate and uniformity, two important microstructure performance measures for the GMR process, as a function of the input variables: power, pressure, gas temperature and electrode spacing. These performance measures, in turn, define well-known device characteristics such as the saturation magnetic field H_{sat} and GMR ratio.[1]

The article is organized as follows. In Sec. II we briefly describe the rf diode sputtering process for metal thin-film fabrication and the reactor-scale models of interest. We then develop and show relevant results for the fluid flow model, the plasma model, the sputter model, and the direct simulation Monte Carlo (DSMC) atom transport model in Secs. III, IV, V, and VI, respectively. A detailed (but slow) integrated, steady-state, input–output model for rf diode sputtering for growing GMR films that results from the integration of these individual model is described in Sec. VII. An approximate input–output ($I-O$) model of rf diode sputtering that provides accurate predictions of process performance several orders-of-magnitude faster than the detailed model is also described in Sec. VII. The approximate model, once it has been refined and validated with experimental data, is shown to be useful for performance sensitivity analysis of deposition rate and uniformity with respect to input power, pressure, temperature, and electrode spacing. Sensitivity results are given in Sec. VII, and in Sec. VIII we show how these sensitivity results can be used to derive set-point control tolerances for the critical thin-film layer in an actual diode-sputtering process. The article concludes in Sec. IX with a summary of the reported work and a brief indication of needed future research.

Due to space limitations we only provide the main equations and, at most, one representative result for each model described below. Detailed development of and extensive results for each of the individual models are documented in Refs. 2 and 3. It is important to note that while commercially available software packages such as SIMBAD and SIMSPUD enable simulation of sputtering and transport processes, the objective of the current work is the development of a more fully integrated model for rf diode sputtering. Specifically, this integrated model includes, in addition to sputter and transport models, a computational fluid dynamical model of gas flow in the chamber, and a capacitative parallel plate rf plasma discharge model for the formation of Ar ions. Also, while the integrated model is currently restricted to an ide-

[a]Electronic mail: desa@scsolutions.com

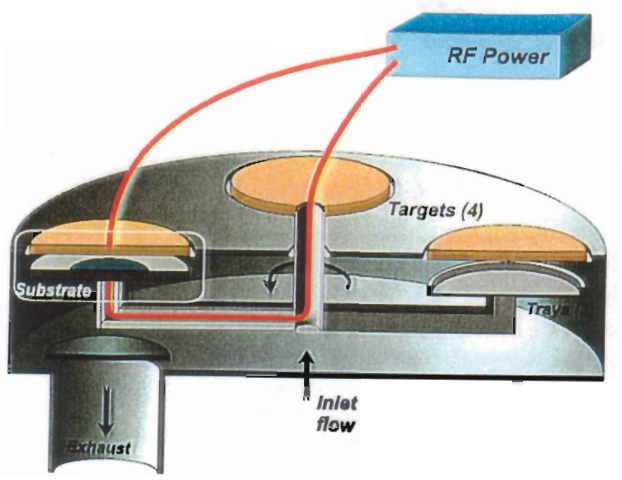

FIG. 1. Schematic depiction of the GMR chamber used by NVE (PE 2400 sputtering system).

ally planar sputter (target) surface, it can be readily extended to handle the case of a contoured sputter surface.

II. rf DIODE SPUTTERING AND DEPOSITION PROCESS

A schematic diagram of the chamber for rf diode sputtering is shown in Fig. 1. The chamber depicted in Fig. 1 represents the essential elements of the Perkins–Elmer PE 2400 sputtering system used by Nonvolatile Electronics (NVE), where the experimental work described herein was performed. We have focused on the sputtering and deposition of copper (Cu), mainly because experimental data for the purposes of model validation was more readily available for Cu thin films. In the fabrication of GMR thin films a variety of targets, for example, CuAgAu and CuNiFe, are used.

The targets for sputtering are mounted at the top while the wafer on which the thin film is deposited is mounted at the bottom of the chamber. (At any given time during the deposition process only the target directly above the substrate is active.) Argon (Ar) gas at low pressure, typically in the range 20–50 mTorr, is pumped into the chamber, and an rf capacitive plasma discharge is generated and maintained between the target electrode and the wafer (substrate) electrode by means of a power supply and rf matching network. Argon ions formed in the plasma bombard the Cu target and sputter (eject) Cu atoms that are then deposited on the wafer substrate.

The proper characterization and quantification of the physical phenomena taking place inside the sputtering chamber requires the following models:

(1) a computational fluid dynamic (CFD) finite element model for the velocity and pressure distribution of the Ar gas flow in the chamber,
(2) a steady-state plasma model for the flux and energy of Ar ions striking the target and the substrate,
(3) a molecular dynamics (MD) sputtering model for the energy distribution, angle distribution, and yield of the Cu atoms sputtered from the target by the Ar ions, and
(4) a binary collision theory (BCT) based DSMC model for the transport of Cu atoms through the low-pressure argon gas to the deposition substrate.

These models will be described in Secs. III–VI

III. FLUID MODEL

The (CFD) finite element model simulates the argon flow in the chamber between the target and substrate and yields the resulting gas velocity and pressure distribution. The finite element analysis was based on well-known continuity, momentum, energy, and state equations for compressible fluid flow given in Ref. 4. For the chamber operating conditions and input flow rates of interest the principal physical equation is the following vector Navier–Stokes momentum equation:

$$\frac{D(\rho \mathbf{V})}{Dt} + \nabla p = \nabla^2(\mu \mathbf{V}) + \mathbf{F}, \tag{3.1}$$

where D/Dt represents the substantial derivative with respect to time t; $\mathbf{V}$, p, and $\mathbf{F}$ are, respectively, the velocity vector, pressure, and the resultant external force vector at a generic point (x,y,z) in the fluid.

Both incompressible and compressible viscous fluid flow models were developed in ADINA-F, a commercial finite element software package, and then used to simulate the gas flow inside the chamber. A representative finite element simulation for the 3D flow field in the region of interest between the target and substrate is shown in Fig. 2.
Based on numerical simulation results such as the one shown in Fig. 2, the maximum magnitude of the gas velocity in the region of interest between the electrodes is approximately 0.01 m/s, and the pressure inside the chamber is approximately constant, with variations of less than 0.01% of the mean pressure. Extensive mesh refinement studies for tetrahedral and hexahedral finite elements as well as for incompressible and compressible flow were performed to establish the convergence of the finite element solutions and therefore the fidelity of the simulations.

The results of the fluid model, i.e., gas pressure and velocity, are used in the plasma model and the transport model as indicated in Sec. VII.

IV. PLASMA MODEL

The primary function of the steady-state plasma model is to predict the flux and energy of argon ions striking the target and the substrate for specified values and ranges of input variables such as applied power and Ar gas pressure.

The input rf power P_{abs} applied to the target electrode a and the substrate electrode b (see Fig. 1), results in the formation of a "bulk" plasma (in the region between the electrodes) containing an equal density n_0 of Ar ions and electrons, with thin "electron-free" regions called sheaths near each electrode. For the range of pressures of interest, 20–50 mTorr, the mean free path of the Ar ions is less than the

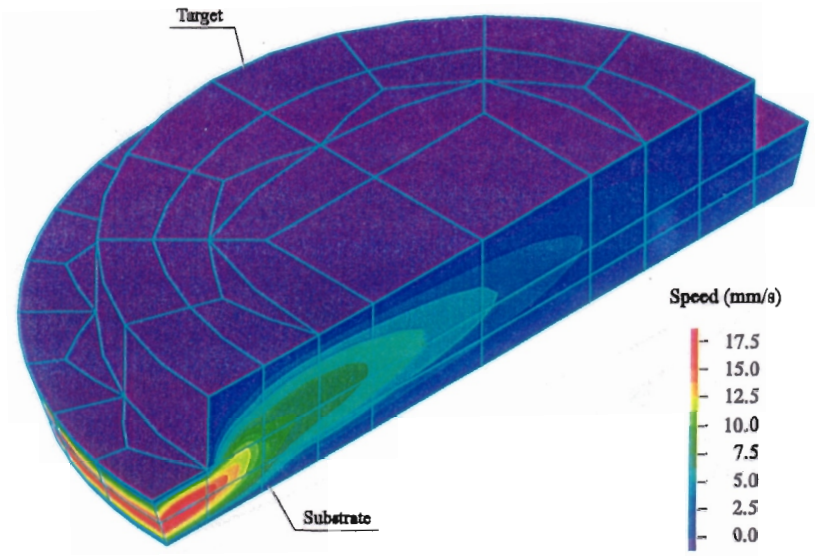

FIG. 2. Flow field between the target and the substrate (CFD model).

sheath thickness, implying that the ions are subject to one or more collisions as they traverse the sheath. For this condition, the sheath is said to be "collisional." Two important variables characterizing the plasma are the thicknesses s_{ma} and s_{mb} and the voltages V_a and V_b of sheath a and sheath b, respectively.

The inputs to the plasma model are as follows: p, the argon gas pressure (Torr) obtained from the fluid model; P_{abs}, the input power (W); l, the distance between electrodes (m); A_a, the target electrode area (m^2); A_b, the substrate electrode area (m^2); T, the gas temperature (K); ω, the rf current frequency (rad/s); and A_s, the substrate area (m^2). Well-known expressions for physical variables of interest in plasma discharge analysis such as the mean free path λ_i of the Ar ions, the electron-neutral Ar collision frequency ν_m, and the ratio (n_s/n_o) of Ar ions at the sheath edge to the Ar ions in the bulk plasma are given in Ref. 5. The so-called "self-consistent" uniform symmetric model for a capacitative parallel-plate rf plasma discharge[5] has been extended to the asymmetric case of unequal target and substrate area as described below. (The simplifying assumptions made in the formulation of the self-consistent model are given in Ref. 5.)

The average sheath voltages $\overline{V_a}$ and $\overline{V_b}$ are related to the areas of the sheath as follows:

$$\gamma \triangleq \overline{V_a}/\overline{V_b} = (A_b/A_a)^q, \tag{4.1}$$

where the exponent q can typically take values between 1.5 and 4 depending on operating conditions.[2,4]

The outputs of interest, the Ar ion flux and the Ar ion energy, are computed from a nonlinear algebraic model based on the three energy balances described below. The first energy balance, accounting for the fact that the rf power P_{abs} supplied to the plasma goes into heating up the plasma, is simply

$$P_{abs} = S_{abs,a}A_a + S_{abs,b}A_b, \tag{4.2}$$

where $S_{abs,a}$ and $S_{abs,b}$ are, respectively, the power loss per unit area corresponding to sheath a and sheath b, and A_b and A_a are, respectively, the areas of sheaths a and b.

The second energy balance relates to the power loss per unit area at each seath $S_{abs,a}$ and $S_{abs,b}$. (The subscripts a and b are omitted below.) For each sheath, E_l, the total energy lost per ion lost from the system, is given by

$$E_l = E_c + 2T_e + E_i, \tag{4.3}$$

where E_c is the collisional energy lost per creation of an electron–ion pair, $2T_e$ is the mean kinetic energy lost per electron striking the electrode (based on a Maxwellian distribution), and E_i is the mean kinetic energy per ion striking the electrode. The ion current density J at each sheath is given by

$$J = en_s u_s, \tag{4.4}$$

where e is the charge on an electron, n_s is the density of Ar ions at the sheath edge, and u_s is the velocity of the ions at the sheath edge. The power loss per unit area S_{abs}, corresponding to each sheath, is given by

$$S_{abs} = JE_l = en_s u_s(E_c + 2T_e + E_i). \tag{4.5}$$

For a collisional sheath

$$E_i = \bar{V} = 0.78V_1, \tag{4.6}$$

where $\bar{V}$ is the average sheath voltage, and V_1 is the peak sheath voltage.

For the third energy balance, we first note that the so-called electron power loss S_e, i.e., that part of the total power loss S_{abs} associated with all collisions involving electrons, is given by

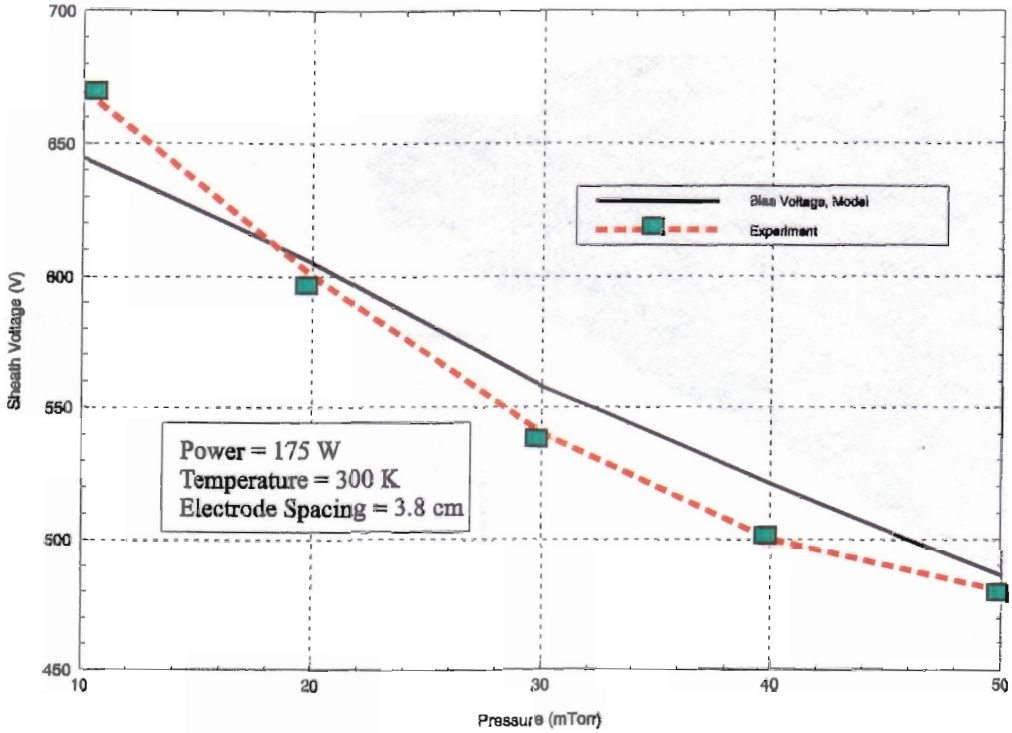

$$S_e = e n_s u_s (E_c + 2T_e), \tag{4.7}$$

where S_e is, in general, due to the following causes: ohmic heating in the bulk plasma $S_{ohm,p}$, ohmic heating in the sheath $S_{ohm,s}$, and stochastic heating in the sheath $S_{stoc,s}$. In terms of these quantities S_e can be expressed as follows:[2]

$$S_e = S_{ohm,p}/2 + S_{ohm,s} + S_{stoc,s}. \tag{4.8}$$

Combining Eqs. (4.5)–(4.8), we obtain the following equation for each sheath:

$$S_{abs} = (S_{ohm,p}/2 + S_{ohm,s} + S_{stoc,s})\left(1 + \frac{\bar{V}}{E_c + 2T_e}\right). \tag{4.9}$$

Equation (4.9) can then be used in Eq. (4.2), once for each sheath. The basic parameters and variables for the plasma discharge enter Eq. (4.2) through highly nonlinear equations for $S_{ohm,p}$, $S_{ohm,s}$, and $S_{stoc,s}$ given (as functions of these variables) in Refs. 2 and 5. The iterative process used to solve for the sheath thicknesses and sheath voltages, Ar ion densities, and Ar ion velocities is documented in Ref. 2.

The output quantities of interest from the plasma model are J, the ion current density, given by Eq. (4.4) and ϵ_{ic}, the energy of the ions when they strike the electrode, given by

$$\epsilon_{ic} = 0.62(\lambda_i/s_m)\bar{V}. \tag{4.10}$$

The steady-state plasma model resulting from the set of highly nonlinear equations described above was coded in XMATH, a commercial package for systems and controls simulation. The plasma model was refined and validated against experimental measurements performed on an actual rf diode sputtering chamber. Figure 3 shows that simulation results for the bias voltage between the electrodes, which is the magnitude of the difference between the two sheath voltages, as a function of pressure, are in close agreement with experimental measurements performed using the NVE chamber. A typical model simulation result from the plasma model (shown in Fig. 4) indicates that increasing the input power significantly increases ion current density (or ion flux). An extensive set of important simulation results, including the effect of power and electrode spacing on ion current density and ion energy, are documented in Refs. 2 and 3. The outputs of the plasma discharge model, the ion current density J and the mean ion impact energy ϵ_{ic}, are the inputs to the sputter model.

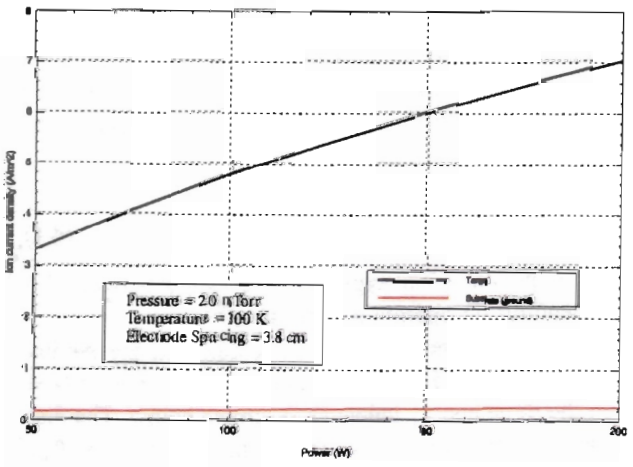

FIG. 4. Effect of power on the ion current density (plasma model).

V. SPUTTER MODEL

When energetic Ar ions bombard a copper target, some of the atoms are sputtered (ejected) from the copper surface. The sputter yield Y and the distribution of the energy ϵ_{Cu} and angle α_{Cu} of the sputtered Cu atoms, as a function of the energy ϵ_i and incident angle θ of the Ar ions striking the target, are computed based on a molecular dynamics sputter model that simulates Ar impacts with the Cu target.[6] (The model also accounts for the effect of the texture of the target surface on the outputs of interest.)

The ion energy ϵ_i is assumed to have the following Rayleigh distribution[2] with mean value ϵ_{ic} equal to the ion energy computed in the plasma model

$$P(x)=xe^{-x^2/2}, \tag{5.1}$$

where $x=\epsilon_i/\epsilon_{ic}$ is the ratio of the incident ion energy to the computed mean ion energy. The sputter yield, $Y(\epsilon_i,\theta)$, i.e., the number of copper atoms sputtered by each argon ion, is given by[2]

$$Y(\epsilon_i,\theta)=\begin{cases}0, & \theta>\theta_m\left(\dfrac{270-\theta_0}{90-\theta_0}\right)^{1/\lambda},\\ a\exp\left[-\left(\dfrac{\alpha}{\epsilon_i}\right)^{\beta}\right]\left\{1+\sin[\theta_0+(90-\theta_0)]\left(\dfrac{\theta}{\theta_m}\right)^{\lambda}\right\}, & \theta<\theta_m\left(\dfrac{270-\theta_0}{90-\theta_0}\right)^{1/\lambda},\end{cases} \tag{5.2}$$

where $\theta_m=50.0°$, $\theta_0=19.9°$, $\lambda=3.23$, $a=3.7$, $\alpha=360.0$, and $\beta=0.85$.

Probability density functions for the energy ϵ_{Cu} and angle α_{Cu} of the sputtered Cu atoms are given in Ref. 2. The Cu atom energy distribution ϵ_{Cu} and angle distribution α_{Cu} are two of the inputs to the transport model described in Sec. VI.

VI. DSMC/BCT TRANSPORT MODEL

An atomistic scale DSMC model based on three-dimensional BCT was developed for simulating the transport of copper atoms inside the low-pressure argon chamber. The BCT code tracks individual metal atoms through the background gas from the sputtering target (source) to deposition substrate with the atom trajectories being determined by binary collisions. The code follows Cu atoms one at a time from the sputtering target to the substrate or out of the modeled volume. During transport modeling, Cu atom collisions with individual "background" Ar gas atoms are simulated at intervals determined from mean free path calculations, with each collision event being treated as an elastic, momentum transferring event that changes the velocity vector of the Cu atom. The model simulates a neutral, monoelemental, monatomic background gas atom interacting with a neutral, monoelemental, monatomic sputtered atom. The physical and computational details of the DSMC/BCT model can be found in Ref. 7. The key calculations of the model, briefly described below, are (a) computation of the mean free path, and (b) calculation of the Cu atom velocity vector following a collision with the background gas atom.

The assumptions associated with the DSMC/BCT model are:

(i) the copper–argon interactions are purely elastic,
(ii) the directed momentum transfer cross section employs the purely repulsive universal potential to describe copper–argon interaction, and
(iii) the background gas atom velocities can be described using a Maxwell–Boltzmann distribution.

The point at which a collision between the sputtered atom and the background gas atom occurs can be determined from a calculation of the atom's mean free path λ which, for an atom traveling in a gas whose velocity distribution follows a Maxwell–Boltzmann distribution, is given by[8,9]

$$\lambda=\frac{RT}{\sqrt{2}pN_A\sigma_d}, \tag{6.1}$$

where R is the universal gas constant (8.3145 J/(mol K)), T is the average carrier gas temperature along the Cu atom's path of travel (K), p is the average carrier gas pressure (obtained from the fluid model) along the Cu atom's path of travel (Pa), N_A is Avogadro's number (6.0221×10^{23} atoms/mol), and σ_d is the directed momentum transfer cross section for the specific gas/sputtered atom combination.

Of the variables included in Eq. (6.1), the directed momentum cross section σ_d is the most challenging to determine.[10–12] An important parameter in the determination of σ_d is χ, the deflection angle for either atom (involved in a binary collision) in the so-called "center-of-mass (CM)" reference frame. The following approximation for σ_d was used:[7]

$$\sigma_d\approx\pi(b_{\max})^2, \tag{6.2}$$

where $b_{\max}$ is defined as the atomic separation at which a Cu–Ar interaction generates an angular deflection χ equal to 0.01 rad. Determination of $b_{\max}$ allows σ_d and in turn λ, the mean free path, for any given collision event energy to be calculated.[7]

The second major calculation of the BCT model involves determination of the Cu atom velocity vector after collision with an argon atom. (The velocity of an Ar atom at any point in the chamber can be obtained from the fluid model.) The velocity vectors of the two atoms prior to the collision event,

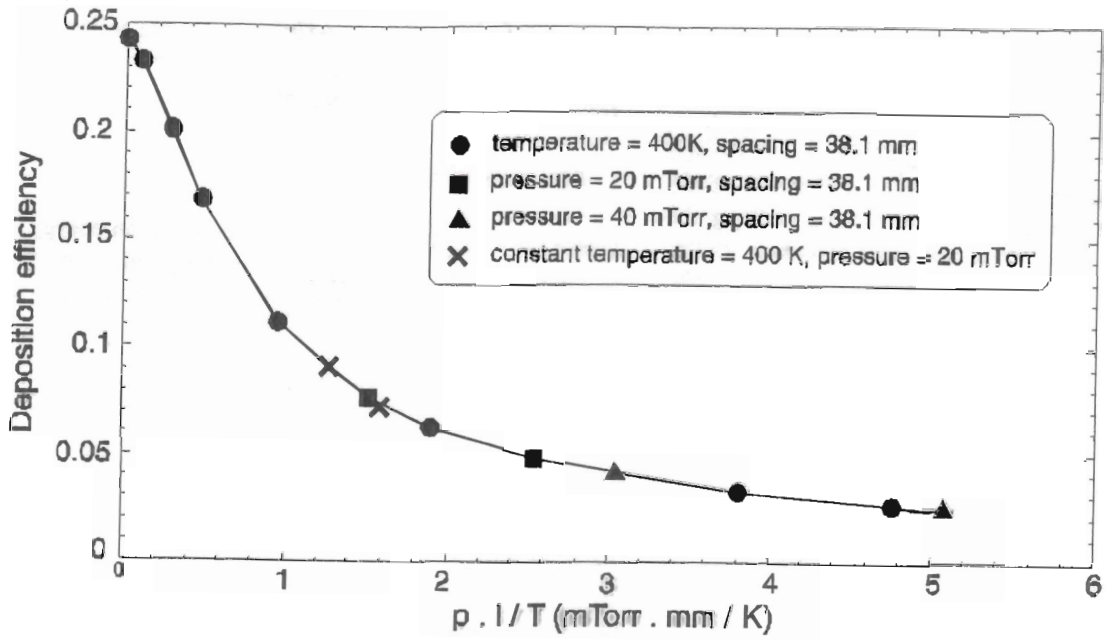

FIG. 5. Deposition efficiency calculated from DSMC transport model.

the relative velocity of those atoms, the mass of the atoms and the form of the interaction potential represent the critical inputs to the well-known "collision" equation given in Ref. 13 describing the velocity vector for the Cu atom after a collision. The difficult part of solving this equation is the determination of the unit vector n_0, the direction of travel of the Cu atom after the collision, which depends upon the interaction potential used. The details of the determination of n_0 are provided in Ref. 7.

One important result of sputter atom transport simulation using the DSMC/BCT model is the deposition efficiency defined as the fraction of the total number of atoms sputtered from the target surface that actually reach the wafer surface. Figure 5 shows that simulation results for different conditions of pressure p, gas temperature T, and electrode spacing l, all lie on a single curve when the deposition efficiency is plotted against a single parameter pl/T. This result can be explained as follows: the deposition efficiency decreases as the number of collisions undergone by the sputter atom increases. The number of collisions is proportional to l, the electrode spacing, as well as to the density of the gas, which in turn is proportional to p/T. Therefore, the number of collisions is proportional to the product of p/T and l, the abscissa of the graph shown in Fig. 5, and as pl/T increases, the deposition efficiency decreases.

Two other important simulation results of the DSMC/BCT model, documented in Ref. 3 are the radial distribution of Cu atoms arriving at the wafer surface, which is a measure of the uniformity of the thin-film deposited on the substrate, and the distribution of energy of the sputter atoms reaching the substrate at various pressures. It is useful to note that at pressures above 10 mTorr, typical for diode sputtering, most of the sputtered atoms reaching the wafer are thermalized.[3]

VII. INTEGRATED FLOW/PLASMA/SPUTTER/TRANSPORT MODEL

The individual models for gas flow, plasma discharge, Cu sputtering, and DSMC based Cu atom transport were integrated to create the detailed virtual integrated prototype (VIP) depicted in Fig. 6, which shows how the various individual models and their respective inputs and outputs are interrelated. Also shown in Fig. 6 are the overall inputs, overall outputs and useful intermediate results of the VIP. A simplified steady-state model was obtained by approximating the results of the fluid, plasma, sputter, and DSMC models with appropriate nonlinear curve fits. This approximate model, coded in *C*, generates the required results in seconds, therefore facilitating quick exploration of the process input–output design space.

The approximate integrated model was refined and validated against experimental results obtained from the NVE chamber. Figure 7 shows that the approximate model yields results for the deposition rate as a function of power, which are in good agreement with experiments. Simulated sensitivity results from the integrated model are shown in Fig. 8 in which the deposition rate is plotted as a function of the main input variables: power, gas pressure, gas temperature and electrode spacing. The results in Fig. 8 show that increasing the input power can significantly increase the deposition rate. Sensitivity results for the effect of the input variables on the film thickness uniformity across the substrate are documented in Refs. 2 and 3.

VIII. SET-POINT CONTROL TOLERANCES

One important application of the approximate integrated *I–O* model, described in this section, is in the determination of the allowable tolerances on the process input variables in

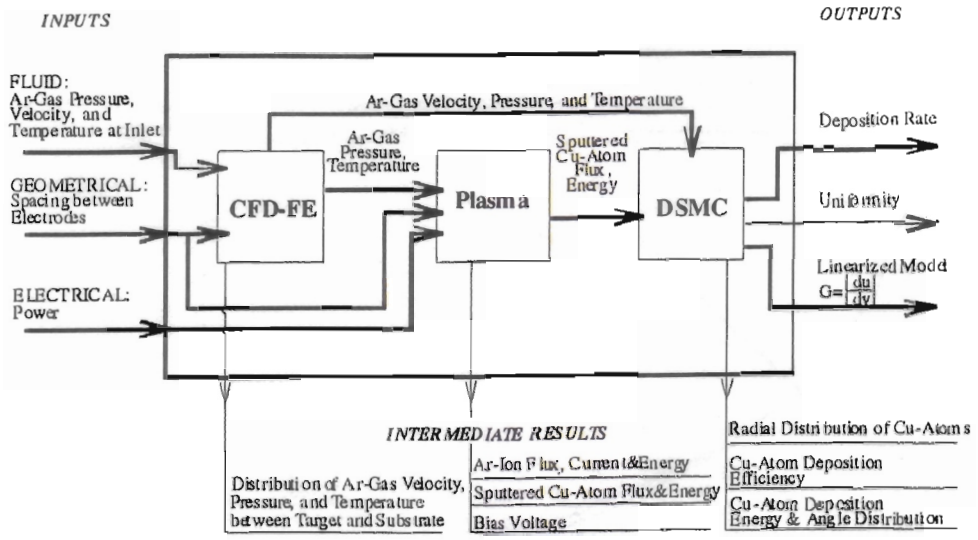

FIG. 6. Virtual integrated prototype for GMR.

order to meet a specified manufacturing tolerance on film thickness. For example, a critical layer in the GMR process is the Cu thin film whose thickness must be 15 Å with a tolerance of 0.25 Å. The nominal deposition rate is 190 Å/min; therefore, a 15 Å layer takes 4.74 s to deposit. The processing time in order to be within the thickness tolerance specifications must be 4.74 ± 0.08 s. Based on the steady-state sensitivities obtained from the plots shown in Fig. 8, the following tolerances (with respect to the nominal values shown) in each input variable will result in a 0.25 Å variation in film thickness in a nominal deposition time of 4.74 s:

power=175 ± 3.50 W (2.0%),

pressure=20 ± 0.28 mTorr (1.4%),

temperature=400 ± 6.2 K (1.6%),

electrode spacing=3.81 ± 0.060 cm (1.6%).

The results of this sensitivity analysis reveal that very small changes in the input process parameters can cause the film thickness to exceed acceptable tolerance limits. Therefore, extremely tight control of inputs such as pressure and power is crucial to maintaining run-to-run repeatability.

IX. CONCLUSION

Reactor models for the principal physical processes involved in rf diode sputtering have been developed and then integrated into a detailed steady-state *I–O* model of the GMR process from gas flow and plasma discharge through sputtering and atom transport to deposition. An approximate model derived from the detailed model was partially validated against experimental data, and then used for performance sensitivity analysis of deposition rate and uniformity with respect to input power, pressure, temperature, and electrode spacing. The use of sensitivity analysis for predicting

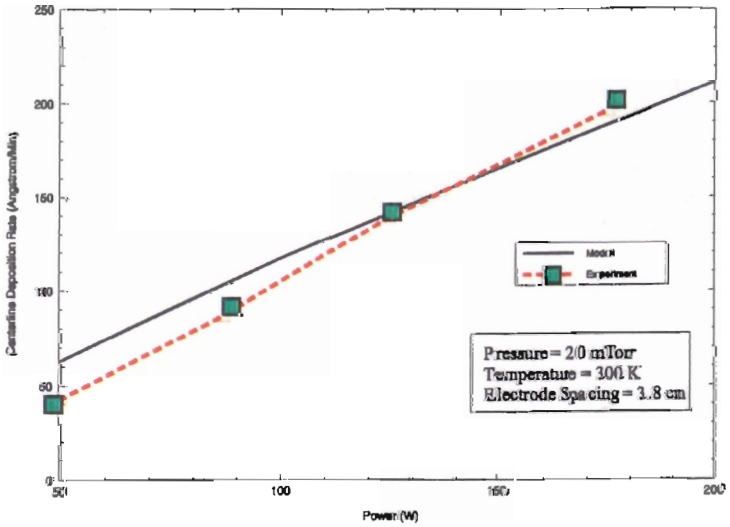

FIG. 7. Experimental validation for deposition rate vs power (integrated model).

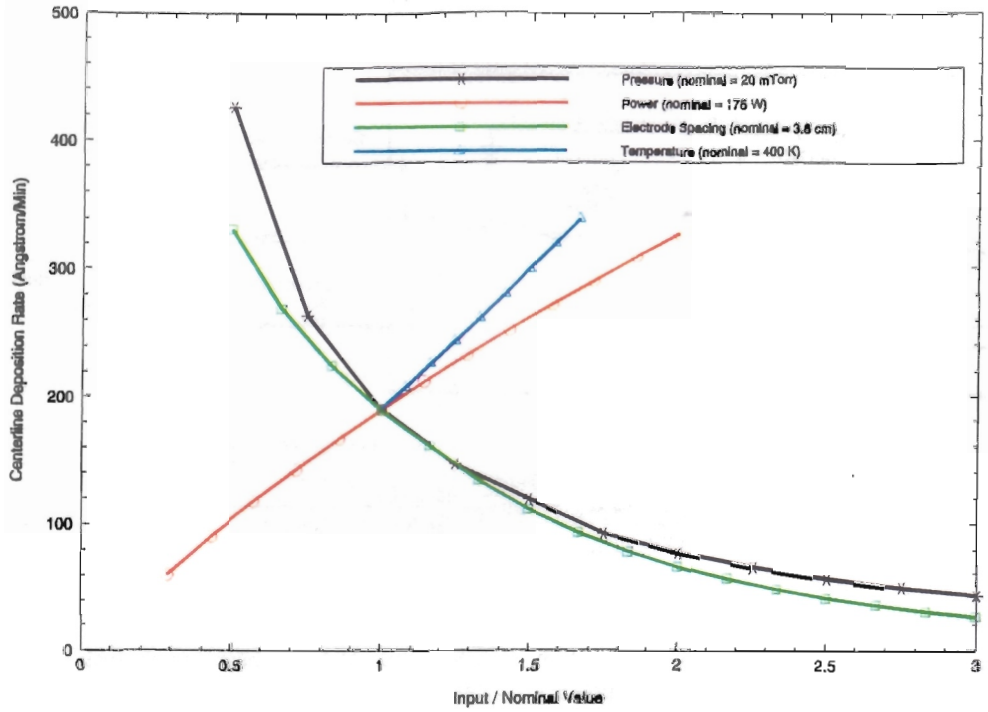

FIG. 8. Sensitivity of deposition rate to the input process variables (integrated model).

control-loop tolerances has been demonstrated. A preliminary rapid VIP of the diode sputtering system has been developed based on the gas flow, plasma, sputtering, and atom transport models. The approximate model and VIP can be used for exploring the $I-O$ operational design space and for feedback and run-to-run control of the process.

Recent and ongoing work in the development and use of reactor models addresses the following issues: a "collisionless" plasma model for gas pressures below 10 mTorr, refinements to the DSMC model, thermal modeling of the chamber to quantify the spatial temperature variations in the chamber, and run-to-run control of deposition rate and uniformity. These issues as well as a more detailed exposition of the models and virtual prototypes described above will be the subject of future papers.

ACKNOWLEDGMENTS

The work presented here was supported by a grant from DARPA, Applied Computation and Mathematics Program. The experimental work was performed at Nonvolatile Electronics (NVE), Eden Prairie, Minnesota.

[1]P. M. Levy, *Giant Magneto-Resistance in Magnetic Layers, Solid-State Physics, Advances in Research and Application* (Academic, San Diego, 1994), Vol. 47.
[2]T. E. Abrahamson, A. Kozak, S. Desa, R. L. Kosut, and J. L. Ebert, SC Solutions Internal Report (December 1997).
[3]R. L. Kosut, T. E. Abrahamson, S. Desa, J. L. Ebert, S. Ghosal, A. Kozak, R. Beech, and D. Wang, SC Report No. GMR-002 (March 1998).
[4]H. Schlichting, *Boundary-Layer Theory*, 7th ed. (McGraw-Hill, New York, 1979).
[5]M. A. Lieberman and A. L. Lichtenberg, *Principles of Plasma Discharges and Materials Processing* (Wiley, New York, 1994).
[6]H. M. Urbassek, Nucl. Instrum. Methods Phys. Res. B 122, 427 (1997).
[7]J. F. Groves, Ph.D. dissertation, University of Virginia, 1998.
[8]E. W. McDaniel, *Collision Phenomena in Ionized Gases* (Wiley, New York, 1964).
[9]G. A. Bird, *Molecular Gas Dynamics and the Direct Simulation of Gas Flows* (Clarendon, New York, 1994).
[10]H. S. W. Massey and E. H. S. Burhop, *Electronic and Ionic Impact Phenomena: Collisions of Electrons with Atoms* (Clarendon, New York, 1969), Vol. I.
[11]R. S. Robinson, J. Vac. Sci. Technol. 16, 185 (1979).
[12]H. S. W. Massey, *Electronic and Ionic Impact Phenomena: Slow Collisions of Heavy Particles* (Clarendon, New York, 1971), Vol. III.
[13]L. D. Landau and E. M. Lifshitz, *Mechanics*, 3rd ed. (Pergamon, New York, 1976).